Magnetic Circular Dichroism of C_{60}^+ and C_{60}^- Radicals in Argon Matrixes

Vaughan S. Langford[†] and Bryce E. Williamson*

Department of Chemistry, University of Canterbury, Private Bag 4800, Christchurch, New Zealand

Received: April 28, 1999; In Final Form: June 14, 1999

Near-infrared transitions of the monoanion and monocation radicals of buckminsterfullerene isolated in argon matrixes ($C_{60}^{\pm}$/Ar) have been investigated using magnetic circular dichroism (MCD) and absorption spectroscopy, over the temperature range $T = 1.6-30$ K and magnetic-field range $B = 0-4$ T. Structure in the origin-band regions of both ions is partially attributed to the occupation of inequivalent matrix sites. The origin bands for the $^2H_g \leftarrow {}^2H_u$ and $^2G_g \leftarrow {}^2H_u$ transitions of C_{60}^+/Ar are nearly coincident, with the former at higher energy. The ground-state orbital angular momenta of both ions are quenched by crystal-field-stabilized Jahn−Teller (CF-JT) effects. Trapping is strong for C_{60}^-/Ar but weak for C_{60}^+/Ar. The transition from static to dynamic CF-JT effects for C_{60}^+/Ar gives rise to unusual temperature and magnetic-field dependencies of the MCD.

I. Introduction

Assuming icosahedral (I_h) symmetry, the near-IR electronic transitions of the monoanion and monocation of C_{60} are assigned, respectively, to $^2T_{1g} \leftarrow {}^2T_{1u}$ [1−3] and ^2H_g, $^2G_g \leftarrow {}^2H_u$.[1,2,4] The terms involved in these transitions are all susceptible to Jahn−Teller (JT) effects, but the magnitudes of JT displacement are predicted to be small.[4−9] For truly isolated ions the effects should be dynamic—in semiclassical terms, rapid tunneling between JT configurations will result in time-averaged retention of the undistorted geometry. In condensed phases, however, dynamic JT effects are susceptible to disruption by crystal fields.[9,10] In effect, relaxation of the local environment can stabilize one JT configuration sufficiently to trap the molecule in a static distortion. On account of the ability of the negative charge of C_{60}^- to polarize the surroundings, Tosatti et al. have predicted that the dynamic effect will be unobservable for C_{60}^- except in the gas phase or, less likely, in inert gas matrixes.[11]

C_{60}^- and C_{60}^+ were first isolated (simultaneously) in an Ar matrix by Gasyna, Andrews, and Schatz.[12] They observed vibronic structure in the overlapping near-IR spectra, which they assigned on the basis of the C_{60} Raman spectrum[13] assuming I_h symmetry. The structure in the origin-band regions of both ions was attributed to combined spin−orbit (SO) and JT effects. An MCD spectrum of C_{60}^-/Ar obtained later by the same workers suggested the presence of a JT overtone shifted by ∼440 cm^{-1} from the origin.[14] Soon afterward, Fulara et al. obtained the absorption spectrum of mass-selected C_{60}^+/Ne at 5 K,[15] which allowed unambiguous identification of vibronic structure in the spectra of both ions. Vibrational assignments were made by assuming a reduction of symmetry from I_h to D_{5d} due to crystal-field-stabilized Jahn−Teller (CF-JT) effects, and the origin-band structure was attributed to matrix sites.

In this paper absorption and temperature- and magnetic-field-dependent MCD data are presented for $C_{60}^{\pm}$/Ar, with the intention of providing further insight into the nature of the JT distortions and crystal-field effects of C_{60}^+ and C_{60}^- in solid inert-gas matrixes.

II. Experimental Section

C_{60}^+ and C_{60}^- were produced simultaneously by using the method of Gasyna et al.[12] C_{60} powder was sublimed in a quartz Knudsen cell at ∼450 °C and then subjected to radiation from a microwave discharge through an 1−2 mmol h^{-1} flow of Ar, which also provided host atoms for the matrix. The photolysis products, Ar and excess C_{60}, were co-condensed onto a cryogenically cooled *c*-cut sapphire window. Data above $T \approx$ 12 K were obtained by using a closed-cycle He refrigerator (APD Cryogenics) placed between the poles of an electromagnet (Alphamagnetics Model 4800).[16] For $T \lesssim$ K an Oxford Instruments SM4 cryomagnet was used in a matrix-injection mode.[17]

MCD and double-beam absorption spectra were measured simultaneously using a spectrometer described previously.[16,18] The 1-m Jarrell-Ash 78−463 monochromator was fitted with a 590-groove mm^{-1} diffraction grating blazed at 1.0 μm. Light was provided by a 250-W tungsten lamp and detected by using a Hamamatsu R-316 photomultiplier tube or Philips BPX-65 Si photodiode. The spectral resolution was ∼0.8 nm.

III. Results

MCD (ΔA) per tesla and absorption (A) spectra for C_{60}^+/Ar and C_{60}^-/Ar, obtained at $T = 12$ K and $B = 0.6$ T using the refrigerator/electromagnet system, are shown in Figure 1. ΔA is the difference between the absorbance of left (A_L) and right (A_R) circularly polarized light by a sample in a longitudinal magnetic field (inductance B), while A is the corresponding average:[19]

$$\Delta A = A_L - A_R \quad (1)$$

$$A = (A_L + A_R)/2 \quad (2)$$

The absorption spectrum is very similar to those reported by Gasyna et al.[12] and Fulara et al.[15] The wavenumbers of the bands

* Corresponding author. E-mail: B.Williamson@chem.canterbury.ac.nz. Fax: ++64 3 364 2110.

[†] Present address: Department of Chemistry, University of Western Australia, Nedlands, Perth, WA 6907, Australia.

10.1021/jp991393v CCC: $18.00
Published on Web 08/03/1999

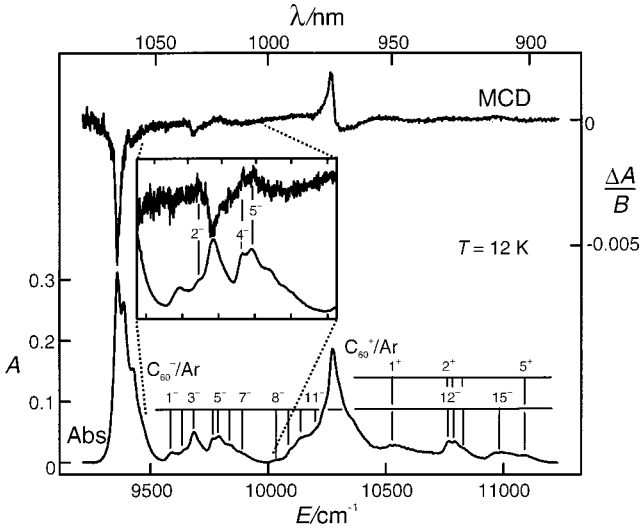

Figure 1. Near-IR MCD per tesla ($\Delta A/B$; top) and absorption (A; bottom) spectra of $C_{60}^{\pm}$/Ar obtained by using the He-refrigerator/electromagnet system at $T = 12$ K and $B = 0.6$ T. The inset shows an expanded view of vibronic structure in the spectra of C_{60}^{-}/Ar. Band numbering is for cross-reference with Table 1.

are summarized in Table 1, where superscripts ± refer respectively to ion charges.

Figure 2 shows expansions from the origin-band regions of the two ions. The lighter spectra are taken from Figure 1, while the darker spectra were obtained at $T = 4.3$ K by using the matrix-injection system. The gross features of the two sets are similar; the MCD for C_{60}^{-}/Ar is single-signed and negative, while for C_{60}^{+}/Ar it is double-signed with the more intense, positive lobe at lower energy. However, the bands obtained by using the matrix-injection apparatus are substantially broader, probably as a consequence of different deposition conditions—whereas the He refrigerator maintained a steady temperature of ~20 K during deposition, the window temperature in the matrix-injection system oscillated between ~12 and 25 K due to the surging of the cryogenic fluid. In support of this conjecture, sharp-band spectra obtained using the refrigerator could be reproducibly transformed into broad-band spectra by annealing above ~25 K.

Spectra were measured at temperatures between $T = 20$ and 1.6 K and magnetic field strengths between $B = 0$ and 4 T. The absorption spectra and the dispersion of the MCD were independent of changes in these conditions. However, the MCD magnitudes showed significant changes, which were quantified by the method of moments.[19] The nth absorption ($\mathbf{A}_n$) and MCD ($\mathbf{M}_n$) moments are given by

$$\mathbf{A}_n = \int \frac{A(E)}{E} (E - \bar{E})^n \, \mathrm{d}E \tag{3}$$

$$\mathbf{M}_n = \int \frac{\Delta A(E)}{E} (E - \bar{E})^n \, \mathrm{d}E \tag{4}$$

where E is the photon energy and $\bar{E}$ is the absorption band barycenter defined by $\mathbf{A}_1 = 0$. $\mathbf{A}_0$ measures the absorption intensity, while $\mathbf{M}_0$ and $\mathbf{M}_1$ reflect the magnitude of various contributions to the MCD (see below).

For quantitative theoretical analysis, the integrals in eqs 3 and 4 are normally carried over all vibrational components of a transition.[19] However, the current situation is complicated by overlap between transitions of the two ions, as well as the weakness and poor signal-to-noise ratio of the MCD. Moment analysis was therefore restricted to the origin-band regions shown in Figure 2.

Rather than unmodified moments, it is convenient to employ ratios of the type $\mathbf{M}_n/\mathbf{A}_0$, which are independent of unknown or poorly characterized parameters such as concentration, path length, and dipole strength. $\mathbf{M}_0/\mu_B B\mathbf{A}_0$ and $\mathbf{M}_1/\mu_B B\mathbf{A}_0$ are plotted against $1/kT$ in Figure 3, while the dependencies of $\mathbf{M}_0/\mathbf{A}_0$ and $\mathbf{M}_1/\mathbf{A}_0$ on $\mu_B B$ are shown in Figure 4 (μ_B is the Bohr magneton and k is Boltzmann's constant). The moment ratios for C_{60}^{-}/Ar show no significant temperature dependence and a have a linear dependence (within experimental error) on magnetic-field strength. The ratios for C_{60}^{+}/Ar, especially $\mathbf{M}_1/\mathbf{A}_0$, show very unusual, nonlinear dependencies on both magnetic-field strength and temperature.

IV. Discussion

Contributions to MCD spectra are conventionally classified as Faraday terms of type A, B and C.[19,20]

A terms arise from first-order Zeeman splittings of the initial and/or final levels of a transition; they are double-signed with a sigmoidal (derivative-shaped) dispersion that contributes to $\mathbf{M}_1$ but not to $\mathbf{M}_0$. They are temperature independent and scale linearly with magnetic-field strength.

B terms represent diamagnetic contributions to the MCD arising from magnetic-field-induced mixing of states. They are also temperature independent and linearly dependent on magnetic-field strength. However, except in the case of accidental near degeneracies, they are generally weak and single signed (positive or negative), contributing to $\mathbf{M}_0$ but not to $\mathbf{M}_1$.

For systems with degenerate ground states the MCD is nearly always (especially at low temperatures) dominated by C terms. These are related to ground-state paramagnetism and exhibit temperature and magnetic-field dependencies that reflect the populations of Zeeman states within the ground-state manifold. When $\mu_B B \ll kT$, the C-term intensity is a linear function of B/T. At higher fields or lower temperatures saturation occurs whereby the absolute intensity increases progressively more slowly with B/T.

In cases where the ground-state orbital angular momentum is substantial, C terms are strong and single signed, giving a large and temperature-dependent contribution to $\mathbf{M}_0$. On the other hand, if the degeneracy is due purely to spin, they are generally much weaker, depending on excited-state SO coupling for their intensity.[19]

C_{60}^{-}/Ar. The near-IR spectrum of C_{60}^{-}/Ar is formally assigned to $^2T_{1g} \leftarrow {}^2T_{1u}$ in I_h symmetry. This transition would be expected to exhibit A and C terms, but the single-signed MCD origin and absence of significant temperature dependence show that the MCD is actually dominated by B terms. The absence of C terms requires that SO interactions and orbital angular momenta of the anion are either intrinsically weak or strongly quenched. These conclusions are commensurate with EPR studies of C_{60}^{-} indicating g values close to the spin-only value,[21−26] and with theoretical expectations of weak SO coupling in C_{60} and its ions.[11,27] The latter militates against the assignment by Gasyna et al. of the origin-band structure in C_{60}^{-}/Ar (and C_{60}^{+}/Ar) to combined JT and SO splittings.[12] A more likely explanation, especially in light of the changes described above on annealing, is that the structure is due to inequivalent matrix sites.[15]

Theoretical calculations by Tosatti et al.[11] indicate that the ground-state orbital angular momentum of isolated C_{60}^{-}should be reduced by dynamic JT effects involving vibrational modes

TABLE 1: Near-IR Bands (cm^{-1}) of C_{60}^-/Ar and C_{60}^+/Ar[a]

	band	this work[b]	Gasyna et al.[12]	Fulara et al.[15]	assignment
C_{60}^-/Ar	0_1^-	9359 (0)	9360	9363	$^2T_{1g} \leftarrow {}^2T_{1u}$ origin; site 1
	0_2^-	9387 (28)	9390		$^2T_{1g} \leftarrow {}^2T_{1u}$ origin; site 2
	0_3^-	9426 (67)	9440		$^2T_{1g} \leftarrow {}^2T_{1u}$ origin; site 3
	0_4^-	9476 sh (117)			$^2T_{1g} \leftarrow {}^2T_{1u}$ origin; site 4
	1^-	9595 sh (236)		9592	
	2^-	9644 sh (285)			JT overtone
	3^-	9686 (327)	9680	9678	
	4^-	9768 (409)			JT overtone
	5^-	9792 (433)	9800	9790	JT overtone
	6^-	9842 (483)			
	7^-	9881 sh (522)		9895	
	8^-	10033 sh (674)			
	9^-	10097 sh (738)			
	10^-	10139 sh (780)	10140	10129	
	11^-	10201 sh (842)			
	12^- [c]	10768 (1409)		10770	
	13^- [c]	10795 (1446)			
	14^- [c]	10834 sh (1485)			
	15^-	10984 br (1635)		10957	
C_{60}^+/Ar	0_1^+	10237 sh (−37)			$^2G_g \leftarrow {}^2H_u$ origin; site 1
	0_2^+	10274 (0)	10280 (0)	10282 (0)	$^2G_g \leftarrow {}^2H_u$ origin; site 2
	0_3^+	10310 sh (36)	10310 (30)		$^2H_g \leftarrow {}^2H_u$ origin; site 1
	0_4^+	10361 (87)	10360 (80)	10355 (73)	$^2H_g \leftarrow {}^2H_u$ origin; site 2
	1^+	10538 br (264)	10540	10526	
	2^+ [c]	10768 (494)		10770	
	3^+ [c]	10795 (521)			
	4^+ [c]	10834 sh (560)			
	5^+	11090 (816)		11090	

[a] Band designations are shown in Figures 1 and 2. Superscripts ± refer to $C_{60}^{\pm}$. [b] Uncertainty in band positions are ±5 cm^{-1}: sh = shoulder; br = broad (0_1^- and 0_2^+). Shifts from the most intense origin bands (0_1^- and 0_2^+) are given in parentheses. [c] Both ions have bands at these wavenumbers.[15]

of h_g symmetry.[9,28] MCD sometimes provides evidence for vibronic activity in the form of alternating signs of the associate vibrational overtones. Theoretical determination of the sign of B terms associated with JT overtones arising from $T_{1u} \otimes h_g$ is complicated, especially since the same vibration may also be active in the excited states. However, it can be readily demonstrated that vibrations that are totally symmetric in I_h symmetry can only give MCD bands with the same sign as the origin. Hence bands 4^-, 5^-, and probably 2^-, which have positive MCD (inset Figure 1), can be confidently assigned to vibronically active vibrational modes. Their shifts from the origin bands (∼420 and ∼285 cm^{-1}; Table 1) accord well with the wavenumbers of ∼432 and ∼265 cm^{-1} obtained from Raman and inelastic neutron scattering data for the h_g modes of C_{60}.[29]

The effective orbital reduction determined by Tosatti et al.[11] is not nearly sufficient in itself to quench C terms to the observed degree. Explication of earlier EPR and the current MCD results almost certainly lies with crystal-field stabilization of a JT distortion,[10] which can cause substantial (and often effectively complete) reduction of orbital angular momenta. Assuming a static CF-JT distortion in the ground state of C_{60}^-/Ar, the spectra are more conveniently discussed in the appropriate subgroup of I_h. The possibilities are D_{5d}, D_{3d}, and D_{2h},[9,30] for which qualitative energy-level diagrams are given in Figure 5. Also illustrated are interlevel Zeeman interactions and allowed transitions referenced to the molecular axes.

Theoretical calculations generally favor a minimum-energy D_{3d} geometry for C_{60}^-,[3,5,8,31,32] but the following analysis is unaffected by the choice of point group. The D_{5d} and D_{3d} cases are equivalent, while D_{2h} may be regarded as formally equivalent since $\mathbf{A}_0$, $\mathbf{M}_0$, and $\mathbf{M}_1$ are independent of unitary transformations of the excited-state basis.[19] Explicit treatment is given for D_{5d}/D_{3d} symmetry. The $^2E_{(1)u} - {}^2A_{2u}$ separation is denoted by Δ, which, to allow for the possibilities of D_{2h} symmetry and different matrix sites having different symmetries and different splittings, is regarded as an effective parameter. It is important to note that Δ is not the vertical separation between electronic hypersurfaces determined by quantum-chemical calculations but refers instead to energy differences between *vibronic* states. These will be substantially smaller than the vertical separations (typically calculated to be several hundred cm^{-1} or greater[5,8,31]) and, in the expectation of weak JT coupling,[4−8] are probably dominated by the crystal-field shifts.

In D_{3d} (D_{5d}) symmetry, the only allowed transition of $^2T_{1g} \leftarrow {}^2T_{1u}$ parentage at low-temperature is $^2E_{(1)g} \leftarrow {}^2A_{2u}$, for which the dipole strength is[19]

$$\bar{D}_0 = \frac{1}{3}\sum_{\alpha} |\langle {}^2E_{(1)g}\, \alpha | \mathbf{m} | {}^2A_{2u} \rangle|^2 \qquad (5)$$

Here, **m** is the electric-dipole moment operator, α is the partner label of the orbitally degenerate excited state, and the bar over D_0 indicates that the parameter is averaged over all possible molecular orientations. The most important contribution to the B-term intensity involves Zeeman interactions between states within the $^2T_{1u}$ manifold, for which the corresponding Faraday parameter is[19]

$$\bar{B}_0 = \frac{2}{3\Delta}\,\mathrm{Im}\sum_{\alpha,\beta} \langle {}^2E_{(1)u}\, \alpha | \mathbf{L} | {}^2A_{2u} \rangle \cdot \langle {}^2A_{2u} | \mathbf{m} | {}^2E_{(1)g} \beta \rangle \times \langle {}^2E_{(1)g} \beta | \mathbf{m} | {}^2E_{(1)u}\, \alpha \rangle \qquad (6)$$

Im indicates the imaginary part of everything to the right and **L** is the orbital angular momentum operator (spin is inconsequential in the absence of significant SO coupling).

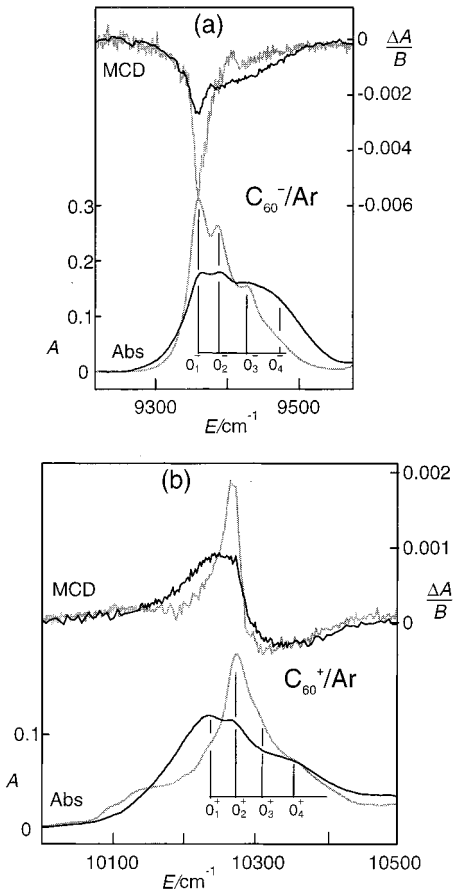

Figure 2. MCD per tesla ($\Delta A/B$; top) and absorption (A; bottom) spectra of the origin-band regions of C_{60}^-/Ar (a) and C_{60}^+/Ar (b). The dark and light spectra respectively illustrate data obtained using the matrix-injection and refrigerator/electromagnet systems. The differences in the spectra are attributed to changes in the occupancies of inequivalent sites due to different deposition conditions. Band numbering is for cross-reference with Table 1.

Matrix elements in the expressions for $\bar{D}_0$ and $\bar{B}_0$ can be inter-related by the Wigner−Eckart theorem after recourse to the I_h parentage of the states (Table 2). The resultant moment ratio is

$$\mathbf{M}_0/\mu_B B\mathbf{A}_0 = \bar{B}_0/\bar{D}_0 = 2\gamma g_{orb}/\Delta \qquad (7)$$

where γ is an effective Ham-reduction factor ($1 \geq \gamma \geq 0$) due to the JT displacements and g_{orb} is the orbital g value for the $^2T_{1u}$ term of the undistorted ion:

$$g_{orb} = \langle {}^2T_{1u}\ 1|L_z|{}^2T_{1u}\ 1\rangle = i\langle {}^2T_{1u}\ x|L_z|{}^2T_{1u}\ y\rangle \qquad (8)$$

Transformation to the $|L\ M_L\rangle$ basis (Table 2), noting the $L = 5$ spherical parentage of the $^2T_{1u}$ states,[33] gives $g_{orb} = -2.5$. Since all other parameters on the right of eq 7 are intrinsically positive, a negative B term is predicted, in agreement with the experimental result (Figures 1 and 2).

Tosatti et al. have provided a theoretical estimate of $\gamma \approx 0.17$,[11] which, when combined the ratio $\mathbf{M}_0/\mu_B B\mathbf{A}_0 = (-1.6 \pm 0.3) \times 10^{-2}$ from Figure 3a, requires $\Delta = 54 \pm 10$ cm^{-1}. The magnitude of this separation is consistent with earlier spectroscopic observations. First, it accounts for the relatively large deviation of the electronic g factors, determined by EPR, from the spin-only value.[21,24] Perturbation theory gives[34]

$$\Delta g = g - g_e \approx -(\gamma g_{orb})^2 \lambda_{SO}/\Delta \qquad (9)$$

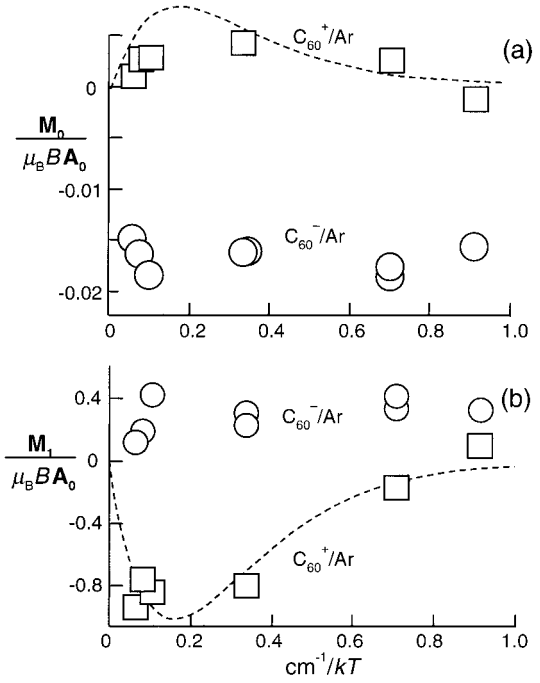

Figure 3. Temperature dependence of the spectroscopic moment ratios $\mathbf{M}_n/\mu_B B\mathbf{A}_0$ obtained by integrating over the ranges of Figure 2: (a) $n = 0$ and (b) $n = 1$. Data for C_{60}^-/Ar are shown as circles, while those for C_{60}^+/Ar are shown as squares. Dashed curves underlying the data for C_{60}^+/Ar were obtained by using eqs 14 and 15, as described in the text.

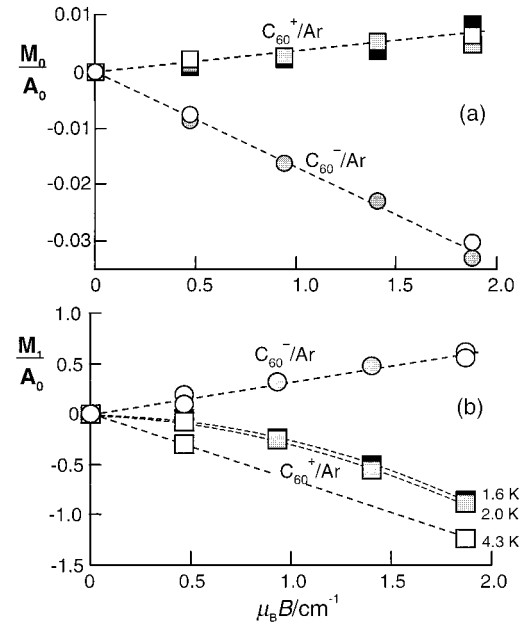

Figure 4. Magnetic-field dependence of the spectroscopic moment ratios $\mathbf{M}_n/\mathbf{A}_0$ obtained by integrating over the ranges of Figure 2: (a) $n = 0$ and (b) $n = 1$. Data for C_{60}^-/Ar are shown as circles, while those for C_{60}^+/Ar are shown as squares. The temperatures at which the data were obtained are coded by the filling of the symbols; black = 1.6 K, gray = 2.0 K, and white = 4.3 K. Dashed curves underlying the data are drawn to guide the eye.

where λ_{SO} is the spin−orbit coupling constant for a t_{1u} electron. The estimate by Tosatti et al.[11] of $\lambda_{SO} = 0.16$ cm^{-1} yields $\Delta g \approx -10^{-3}$, a factor of 2 or 3 smaller than observed shifts but, given the inherent uncertainties of the theoretical estimates, in reasonable accord with experiment.[21−26] In comparison, Nakagawa et al. analyzed Δg for C_{60}^- in methylene chloride to obtain

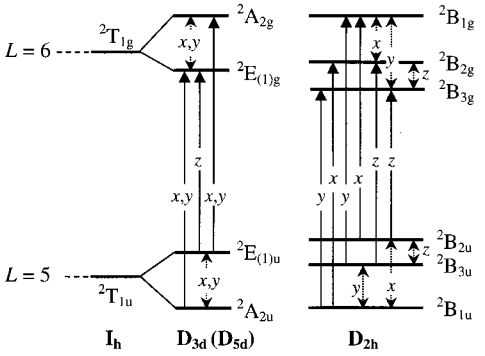

Figure 5. Correlation diagram for reduction from I_h to D_{3d}, D_{5d}, and D_{2h} symmetries for the $^2T_{1g} \leftarrow {}^2T_{1u}$ transition of C_{60}^-. Allowed transitions (full arrows) and inter-level Zeeman interactions (dashed arrows) are referenced to the molecular axes. Energy orderings follow refs 3, 32, and 8.

$\Delta \approx 70$ cm^{-1}.[21] Second, EPR temperature dependence[22,23,35] and features observed in the near-IR absorption spectra of C_{60}^- in benzonitrile[36] have been attributed to the presence of low-lying thermally accessible $^2E_{(1)u}$ excited states. Population of these states should also confer MCD temperature dependence (see below), but with $\Delta \gtrsim 50$ cm^{-1} such effects will be imperceptible at the temperatures of our experiments.

The presence of inequivalent matrix sites and limitation of range of integration to the origin-band region will compromise the reliability of $\mathbf{M}_1$, so interpretation of the ratio $\mathbf{M}_1/\mathbf{A}_0$ is necessarily qualitative. For $^2E_{(1)g} \leftarrow {}^2A_{2u}$ (in the limit of weak SO coupling), $\mathbf{M}_1$ arises from an A term associated with the formal orbital degeneracy of the excited state. The corresponding Faraday parameter is[19]

$$\bar{A}_1 = \frac{i}{3}\sum_{\alpha,\beta}\langle {}^2E_{(1)g}\,\alpha|\mathbf{L}|{}^2E_{(1)g}\,\beta\rangle\cdot\langle {}^2A_{2u}|\mathbf{m}|{}^2E_{(1)g}\,\alpha\rangle \times \langle {}^2E_{(1)g}\beta|\mathbf{m}|{}^2A_{2u}\rangle \quad (10)$$

Table 2 and the Wigner−Eckart theorem then give,

$$\mathbf{M}_1/\mu_B B\mathbf{A}_0 = \bar{A}_1/\bar{D}_0 = \gamma' g'_{orb} \quad (11)$$

where g'_{orb} and γ' now pertain to the excited state. The $L = 6$ parentage of the $^2T_{1g}$ states (Table 2) gives $g'_{orb} = 0.5$; hence the A term is predicted to be positive, in accord with the experimental value of $\mathbf{M}_1/\mu_B B\mathbf{A}_0 = 0.30 \pm 0.15$ (Figure 3b). Although this value must be treated with caution, the estimate of $\gamma' = 0.6 \pm 0.3$ that it gives suggests that the excited-state JT displacements are much smaller than those in the ground state.

C_{60}^+/Ar. The situation for C_{60}^+/Ar is more complicated, in terms of both experimentally observed behavior and its theoretical treatment. The undistorted cation has a ^2H_g ground-state term arising from a vacancy in the h_u ($l = 5$) HOMO.[1,2,4] The near-IR spectra are attributed to transitions $^2H_g \leftarrow {}^2H_u$ and $^2G_g \leftarrow {}^2H_u$, involving excitations to the HOMO from lower-lying h_g and g_g ($l = 4$) orbitals.[1,2,4,15] These transitions are predicted to have similar intensities and to lie within a few hundred cm^{-1} of each other.[1,2,4] The absence of strong C_{60}^+ bands outside the range of Figure 2b, suggests that the origins of both transitions fall within this region.

In the absence of a symmetry-lowering mechanism, the MCD should be dominated by oppositely signed C terms with an intensity ratio of ~16:7, the $^2G_g \leftarrow {}^2H_u$ contribution being positive and stronger. The MCD of the origin-band region (Figures 1 and 2b) is qualitatively consistent with these expectations, but there are three problems. First, the $\mathbf{M}_0/\mathbf{A}_0$ ratios (Figure 3a) obtained by integrating over the range of Figure 2b are at least 2 orders of magnitude weaker than expected for the sum of the two transitions in I_h symmetry. Second, the observed magnetic-field and temperature dependencies are highly unusual, the latter being the exact opposite of the expected $1/T$ behavior for C terms.[19] And third, the energy order (positive MCD band at lower energy) contradicts calculations that put ^2G_g at higher energy.[1,2,4]

The weak MCD clearly indicates that the ground-state orbital angular momentum of C_{60}^+/Ar is quenched, presumably again by CF-JT effects, but now involving vibrations of h_g and g_g symmetries.[9] Bendale et al., using an INDO/S calculation, have found that the most-stable C_{60}^+ structure has D_{5d} symmetry,[4] the energy-level diagram for which is given in Figure 6. The situation is more complex than for C_{60}^-. For example, the multitude of Zeeman interactions provides far greater potential for B terms, particularly if the $^2H_g-{}^2G_g$ separation is small enough to allow significant inter-term Zeeman effects. However, a model that assumes pure B terms associated with transitions from the $^2A_{1u}$ state cannot even begin to account for the unusual temperature and magnetic-field dependencies. The only reasonable explanation requires thermal population of states within a few cm^{-1} of the low-symmetry ground state, in which case the possibility must be allowed for (quasi) C terms associated with transitions from the (formally) orbitally degenerate ^2E levels.

Unfortunately, the available information is insufficient to disentangle the problem within the framework of Figure 6.

TABLE 2: $|L\ M_L\rangle$ Parentage for $C_{60}^{\pm}$ States in I_h and D_{5d} Symmetries[a]

		orbital function		
ion	term	I_h	D_{5d}	$\|L\ M_L\rangle$ parentage
C_{60}^-	$^2T_{1u}$	$\|T_{1u}\,0\rangle$	$\|A_{2u}\rangle$	$(7/50)^{1/2}(\|5\ 5\rangle - \|5{-}5\rangle) - (36/50)^{1/2}\|5\ 0\rangle$
		$\|T_{1u}\,\pm1\rangle$	$\|E_{1u}\,\pm1\rangle$	$-(3/10)^{1/2}\|5\pm1\rangle \mp (7/10)^{1/2}\|5\mp4\rangle$
	$^2T_{1g}$	$\|T_{1g}\,0\rangle$	$\|A_{2g}\rangle$	$-(1/2)^{1/2}(\|6\ 5\rangle + \|6{-}5\rangle)$
		$\|T_{1g}\,\pm1\rangle$	$\|E_{1g}\,\pm1\rangle$	$-(6/50)^{1/2}\|6\pm6\rangle \pm (33/50)^{1/2}\|6\pm1\rangle + (11/50)^{1/2}\|6\mp4\rangle$
C_{60}^+	^2H_u	$\|H_u\,0\rangle$	$\|A_{1u}\rangle$	$-(1/2)^{1/2}(\|5\ 5\rangle + \|5{-}5\rangle)$
		$\|H_u\,\pm1\rangle$	$\|E_{1u}\,\pm1\rangle$	$-(7/10)^{1/2}\|5\pm1\rangle \pm (3/10)^{1/2}\|5\mp4\rangle$
		$\|H_u\,\pm2\rangle$	$\|E_{2u}\,\pm2\rangle$	$\pm(2/5)^{1/2}\|5\pm2\rangle + (3/5)^{1/2}\|5\mp3\rangle$
	^2H_g	$\|H_g\,0\rangle$	$\|A_{1g}\rangle$	$-\|4\ 0\rangle$
		$\|H_g\,\pm1\rangle$	$\|E_{1g}\,\pm1\rangle$	$\pm(8/15)^{1/2}\|4\pm1\rangle \pm (7/15)^{1/2}\|4\mp4\rangle$
		$\|H_g\,\pm2\rangle$	$\|E_{2g}\,\pm2\rangle$	$-(1/15)^{1/2}\|4\pm2\rangle \mp (14/15)^{1/2}\|4\mp3\rangle$
	^2G_g	$\|G_g\,\pm1\rangle$	$\|E_{1g}\,\pm1\rangle$	$\mp(7/15)^{1/2}\|4\pm1\rangle + (8/15)^{1/2}\|4\mp4\rangle$
		$\|G_g\,\pm2\rangle$	$\|E_{2g}\,\pm2\rangle$	$-(14/15)^{1/2}\|4\pm2\rangle \pm (1/15)^{1/2}\|4\mp3\rangle$

[a] Basis functions conform to Butler's conventions for the point-group chain $O_3 \supset I_h \supset D_{5d} \supset C_{5i}$.[30] Relationships for the alternative chains, $O_3 \supset I_h \supset D_{3d} \supset C_{3i}$ and $O_3 \supset I_h \supset T_h \supset D_{2h} \supset C_{2i}$, can be derived from tables in ref 30.

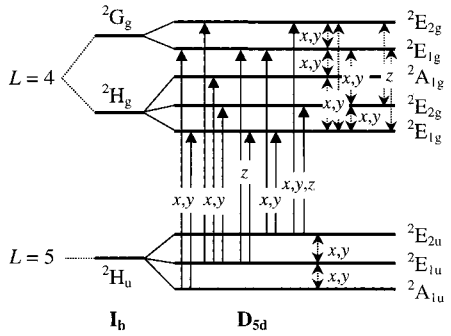

Figure 6. Correlation diagram for reduction from I_h to D_{5d} symmetry for the $^2H_g \leftarrow {}^2H_u$ and $^2G_g \leftarrow {}^2H_u$ transitions of C_{60}^-. Allowed transitions (full arrows) and inter-level Zeeman interactions (dashed arrows) are referenced to the molecular axes. Energy orderings follow ref 4.

Instead, we resort to a phenomenological model in which the system reverts to the high-symmetry situation when the thermal energy exceeds the ground-state CF-JT splittings. At very low temperatures the molecules are trapped in the low-symmetry structure and C terms are entirely quenched. Their reappearance with increasing temperature is modeled by an effective activation energy E_a, which should be similar to the separations between states within the ^2H_u manifold.

As stated above, transitions $^2H_g \leftarrow {}^2H_u$ and $^2G_g \leftarrow {}^2H_u$ in I_h symmetry should have oppositely signed C terms. Hence, bands 0_1^+ and 0_3^+ are assigned to opposite-signed origins of a lower-energy site, and 0_2^+ and 0_4^+ to the origins of a higher-energy site. According to Table 1, the separation between the two excited states is therefore $\sim$80 cm^{-1}. The (orientation-independent) dipole strengths are given by[19]

$$D_0(^2\Gamma_g) = \frac{1}{10}\sum_{\gamma\alpha}(|\langle ^2\Gamma_g\gamma|m_{+1}|^2H_u\,\alpha\rangle|^2 + |\langle ^2\Gamma_g\,\gamma|m_{-1}|^2H_u\,\alpha\rangle|^2) \quad (12)$$

where Γ = H or G and the matrix elements of m_{+1} and m_{-1} are, respectively, left- and right-circularly polarized transition moments ($m_{\pm1} = \mp 2^{-1/2}(m_x \pm im_y)$). The corresponding C-term Faraday parameters are[19]

$$C_0(^2\Gamma_g) = \frac{-1}{10}\sum_{\gamma\alpha}\langle ^2H_u\,\alpha|L_z|^2H_u\,\alpha\rangle(|\langle ^2\Gamma_g\,\gamma|m_{+1}|^2H_u\,\alpha\rangle|^2 - |\langle ^2\Gamma_g\,\gamma|m_{-1}|^2H_u\,\alpha\rangle|^2) \quad (13)$$

and temperature dependencies of the moment ratios are given by

$$\mathbf{M}_0/\mu_B B\mathbf{A}_0 = \frac{e^{-E_a/kT}}{kT}\left(\frac{C_0(^2H_g) + C_0(^2G_g)}{D_0(^2H_g) + D_0(^2G_g)}\right) = -3\gamma g_{orb}\, e^{-E_a/kT}/5kT \quad (14)$$

$$\mathbf{M}_1/\mu_B B\mathbf{A}_0 = \frac{[\bar{E}(^2G_g) - \bar{E}(^2H_g)]e^{-E_a/kT}}{kT} \times \frac{[C_0(^2G_g)\,D_0(^2H_g) - C_0(^2H_g)\,D_0(^2G_g)]}{[D_0(^2H_g) + D_0(^2G_g)]^2} = -168\gamma g_{orb}\, e^{-E_a/kT}\,[\bar{E}(^2G_g) - \bar{E}(^2H_g)]/225kT \quad (15)$$

where γ and g_{orb} pertain to the ^2H_u ground-state term. From the $L = 5$ parentage of the term (Table 2),[33]

$$g_{orb} \equiv \langle ^2H_u\,1|L_z|^2H_u\,1\rangle = -0.5 \quad (16)$$

The best fit of eq 15 to the experimental temperature-dependence data is shown by the dashed curve in Figure 3b. With $|\bar{E}(^2G_g) - \bar{E}(^2H_g)| = 80 \pm 10$ cm^{-1}, it yields $\gamma = 0.58 \pm 0.13$ and $E_a = 6.2 \pm 1.2$ cm^{-1}. Since γ is inherently positive, the negative values of $\mathbf{M}_1/\mu_B B\mathbf{A}_0$ require the ^2H_g term to lie at a higher energy than ^2G_g.

These parameters and eq 14 give the calculated curve for $\mathbf{M}_0/\mu_B B\mathbf{A}_0$ shown at the top of Figure 3a. The model is too crude to expect an accurate fit to the experimental data, but the sign and magnitude of the calculated ratio, and the general form of its temperature dependence, are sufficient to suggest that the model has qualitative validity. This immediately suggests that JT-CF effects in the ground state of C_{60}^+/Ar are far weaker than for C_{60}^-/Ar, a conclusion that is substantiated by both the much larger value of γ and the small value of E_a.

Weak JT-CF effects are also consistent with the nonlinear dependence of $\mathbf{M}_1/\mathbf{A}_0$ on magnetic-field strength at low temperatures (Figure 4b). At weak fields ($\mu_B B \lesssim 0.5$ cm^{-1}) the C terms are strongly quenched. As the field is increased, the lowest CF-JT state progressively takes the character of the lowest Zeeman component of the undistorted ^2H_u term (in a manner analogous to the Paschen−Back effect) and the C terms reappear. This process involves magnetic-field-induced mixing of the $^2A_{1u}$ and $^2E_{iu}$ states via L_x and L_y, the same mechanism that is responsible for B terms. However, the conventional treatment of B terms requires inter-state zero-field separations to be large compared with their Zeeman interactions so that first-order perturbation theory is appropriate. As the magnitudes of the Zeeman interactions approach the splittings, higher-order terms in the perturbation expansion become important and the field dependence becomes nonlinear. $\mathbf{M}_0/\mathbf{A}_0$ should show similar nonlinear magnetic-field dependence, but the signal-to-noise ratio of the experimental data is too poor to verify this expectation.

V. Conclusion

Absorption and MCD spectra have been measured at several temperatures and magnetic fields for the near-IR transitions of $C_{60}^-$and C_{60}^+ in solid Ar. On the basis of annealing behavior, the structure in the origin-band regions of both ions is attributed partially to the occupation of inequivalent matrix sites. For C_{60}^+, some of the structure is ascribed to nearly coincident transitions of $^2H_g \leftarrow {}^2H_u$ and $^2G_g \leftarrow {}^2H_u$ parentage. Positive MCD bands in the vibrational overtone region of the $^2T_{1g} \leftarrow {}^2T_{1u}$ spectrum of C_{60}^- are assigned to a Jahn−Teller-active h_g modes with wavenumbers of $\sim$285 and $\sim$420 cm^{-1}.

For the $^2T_{1g} \leftarrow {}^2T_{1u}$ transition of C_{60}^-/Ar, the single-signed MCD, its temperature independence and linear magnetic-field dependence are commensurate with B terms whose existence can be rationalized in terms of crystal-field-stabilized Jahn−Teller (CF-JT) effects in the ground state. Semiquantitative analysis of the zeroth moments is consistent with effective D_{5d} or D_{3d} symmetry, with a ground-state vibronic splitting of $\gtrsim$50 cm^{-1}. These conclusions are in accord with g values obtained previously by using EPR.[21−26] The first MCD moment suggests significant but smaller JT displacements of the excited states.

The MCD of C_{60}^+/Ar exhibits very unusual temperature and magnetic-field dependencies. It is proposed that the ground state is split by CF-JT effects to give low-lying excited states that are thermally accessible even at liquid-helium temperature. The

magnitude of the JT distortion is weak and the system undergoes a transition between crystal-field-stabilized static and dynamic JT effects, which is responsible for the unusual behavior. The two-signed MCD near 10 250 cm^{-1} indicates that the $^2H_g \leftarrow {}^2H_u$ and $^2G_g \leftarrow {}^2H_u$ origins are separated by only ~80 cm^{-1}, with the former at higher energy. The separation is similar to those found by Fulara et al. in absorption spectra of C_{60}^+/Ar (87 cm^{-1}) and C_{60}^+/Ne (67 cm^{-1}),[15] but the energy ordering is the reverse of predictions obtained by using molecular-orbital calculations.[1,2,4]

The current work has implications with regard to the intriguing theoretical results recently obtained by Tosatti et al.[11] They predicted that the combination of very weak SO coupling and dynamic JT effects in the ground-state term of C_{60}^- should result in an uncommonly strong magnetic-field dependence of the *g* values and a transition from paramagnetism to effective diamagnetism as the temperature is decreased below ~0.2 K. As foreseen by those workers, crystal-field stabilization of the JT effect in the ground state of C_{60}^-/Ar makes that system unsuitable for testing their predictions. However, much weaker trapping in the case of C_{60}^+/Ar would make the cationic system a prime alternative candidate for investigation by EPR. Indeed, our interpretation of the MCD effectively represents a transition from paramagnetism to diamagnetism with decreasing temperature, but the transition is shifted to higher temperature due to the influence of weak crystal fields.

Acknowledgment. We thank Prof. Paul Schatz and Dr. Zbigneiw Gasyna for supplying us with unpublished 5-K absorption and MCD data for C_{60}^-/Ar and C_{60}^+/Ar.

References and Notes

(1) Kato, T.; Kodama, T.; Shida, T.; Nakagawa, T.; Matsui, T.; Suzuki, S.; Shiromaru, H.; Yamauchi, K.; Achiba, Y. *Chem. Phys. Lett.* **1991**, *180*, 446−450.

(2) Heath, G. A.; McGrady, J. E.; Martin, R. L. *J. Chem. Soc., Chem. Commun.* **1992**, 1272−1274.

(3) Lawson, D. R.; Feldheim, D. L.; Foss, C. A.; Dorhout, P. K.; Elliot, C. M.; Martin, C. R.; Parkinson, B. *J. Electrochem. Soc.* **1992**, *139*, L68-L71.

(4) Bendale, R. D.; Stanton, J. F.; Zerner, M. C. *Chem. Phys. Lett.* **1992**, *194*, 467−471.

(5) Koga, N.; Morokuma, K. *Chem. Phys. Lett.* **1992**, *196*, 191−196.

(6) Wang, W.-Z.; Bishop, A. R.; Yu, L. *Phys. Rev. B* **1994**, *50*, 5016−5019.

(7) Borshch, S. A.; Prassides, K. *J. Phys. Chem.* **1996**, *100*, 9348−9351.

(8) Green, W. H. J.; Gorun, S. M.; Fitzgerald, G.; Fowler, P. W.; Ceulemans, A.; Titeca, B. C. *J. Phys. Chem.* **1996**, *100*, 14892−14898.

(9) Chancey, C. C.; O'Brien, M. C. M. *The Jahn−Teller Effect in C_{60} and Other Icosahedral Complexes*; Princeton University Press: Princeton, NJ, 1997.

(10) Englman, R. *The Jahn−Teller Effect in Molecules and Crystals*; Wiley-Interscience: London, 1972.

(11) Tosatti, E.; Manini, N.; Gunnarsson, O. *Phys. Rev. B* **1996**, *54*, 17184−17190.

(12) Gasyna, Z.; Andrews, L.; Schatz, P. N. *J. Phys. Chem.* **1992**, *96*, 1525−1527.

(13) Bethune, D. S.; Meijer, G.; Tang, W. C.; Rosen, H. J.; Golden, W. G.; Seki, H.; Brown, C. A.; de Vries, M. S. *Chem. Phys. Lett.* **1991**, *179*, 181−186.

(14) Gasyna, Z.; Schatz, P. N. Private communication.

(15) Fulara, J.; Jakobi, M.; Maier, J. P. *Chem. Phys. Lett.* **1993**, *211*, 227−234.

(16) Langford, V. S.; Williamson, B. E. *J. Phys. Chem. A* **1997**, *101*, 3119−3124.

(17) Dunford, C. L.; Williamson, B. E. *J. Phys. Chem. A* **1997**, *101*, 2050−2054.

(18) Langford, V. S. Ph.D. Dissertation, University of Canterbury, Christchurch, 1997.

(19) Piepho, S. B.; Schatz, P. N. *Group Theory in Spectroscopy with Applications to Magnetic Circular Dichroism*; Wiley-Interscience: New York, 1983.

(20) Buckingham, A. D.; Stephens, P. J. *Annu. Rev. Phys. Chem.* **1966**, *17*, 399−432.

(21) Kato, T.; Kodama, T.; Oyama, M.; Okazaki, S.; Shida, T.; Nakagawa, T.; Matsui, Y.; Suzuki, S.; Shiromaru, H.; Yamanauchi, K.; Achiba, Y. *Chem. Phys. Lett.* **1991**, *186*, 35−39.

(22) Dubois, D.; Jones, M. T.; Kadish, K. M. *J. Am. Chem. Soc.* **1992**, *114*, 6446−6451.

(23) Schell-Sorokin, A. J.; Mehran, F.; Eaton, G. R.; Eaton, S. S.; Viehbeck, A.; O'Toole, T. R.; Brown, C. A. *Chem. Phys. Lett.* **1992**, *195*, 225−231.

(24) Kato, T.; Kodama, T.; Shida, T. *Chem. Phys. Lett.* **1993**, *205*, 405−409.

(25) Bennati, M.; Grupp, A.; Bauerle, P.; Mehring, M. *Chem. Phys.* **1994**, *185*, 221−227.

(26) Stasko, A.; Brezova, V.; Rapta, P.; Asmus, K.-D.; Guldi, D. M. *Chem. Phys. Lett.* **1996**, *262*, 233−240.

(27) Adrian, F. J. *Chem. Phys.* **1996**, *211*, 73−80.

(28) Dunn, J. L.; Bates, C. A. *Phys. Rev. B* **1995**, *52*, 5996−6005.

(29) Schettino, V.; Salvi, P. R.; Bini, R.; Cardini, G. *J. Chem. Phys.* **1994**, *101*, 1079−11081.

(30) Butler, P. H. *Point Group Symmetry Applications*; Plenum Press: New York, 1981.

(31) Tanaka, K.; Okada, M.; Okahara, K.; Yamabe, T. *Chem. Phys. Lett.* **1992**, *193*, 101−103.

(32) Kondo, H.; Momose, T.; Shida, T. *Chem. Phys. Lett.* **1995**, *237*, 111−114.

(33) Savina, M. R.; Lohr, L. L.; Francis, A. H. *Chem. Phys. Lett.* **1993**, *205*, 200−206.

(34) Weltner, W. J. *Magnetic Atoms and Molecules*; Dover Publications: Mineola, NY, 1989.

(35) Stinchcombe, J.; Penicaud, A.; Bhyrappa, P.; Boyd, P. D. W.; Reed, C. A. *J. Am. Chem. Soc.* **1993**, *115*, 5212−5217.

(36) Bolskar, R. D.; Gallagher, S. H.; Armstrong, R. S.; Lay, P. A.; Reed, C. A. *Chem. Phys. Lett.* **1995**, *247*, 57−62.